Chapter 5

Interface Fluxes and Riemann Solvers

In chapter 3 we described how any basic cell-centred scheme that integrates the equations of fluid motion using a quasi-rectangular mesh could be routinely incorporated into the AMR algorithm. We shall now describe one such method, Roe's flux-difference splitting scheme.

Roe's method belongs to a class of characteristic based schemes that have been developed from the ideas of Godunov[29]. These schemes have proved to be very successful in calculating one-dimensional flows with strong shocks. The robustness of these schemes is due to the physical information embodied within a Riemann problem, and so we shall start with a brief description of Riemann problems and how they may be used to calculate fluxes at cell interfaces. Details will then be given on how Roe's approximate Riemann solver may be extended to multi-dimensions. The basic scheme can sometimes lead to false results, details are given as to what *fixes* may be applied to prevent this from happening. Much of the information presented in this chapter is not specific to Roe's approximate Riemann solver, wherever appropriate attention is drawn to the wider applicability of a result.

5.1 Riemann Problems

A Riemann problem $(\mathbf{W_L}, \mathbf{W_R})$ arises if initial data is prescribed as two semi-infinite states,

$$\begin{aligned} \mathbf{W} &= \mathbf{W_L} \qquad \text{for } x < 0 \\ \mathbf{W} &= \mathbf{W_R} \qquad \text{for } x > 0. \end{aligned} \tag{5.1}$$

The solution to the one-dimensional Euler equations for this initial data consists of three centred waves separating four states $\mathbf{W_L}, \mathbf{W_L^*}, \mathbf{W_R^*}$ and $\mathbf{W_R}$, see figure 5.1. The inner wave is a contact discontinuity separating states of different density, while each of the two other waves may be either a shock wave or an expansion wave. For the Euler equations no closed form analytic solution exists to the Riemann problem. However, by recognising that there is no change in pressure P or velocity U across the contact discontinuity, that is $P_L^* = P_R^*$ and $U_L^* = U_R^*$, we may derive a set of algebraic equations that may then be solved iteratively to find P^*. From which we can then find U^*, ρ_L^* and ρ_R^*. Full details of this process may be found in[32].

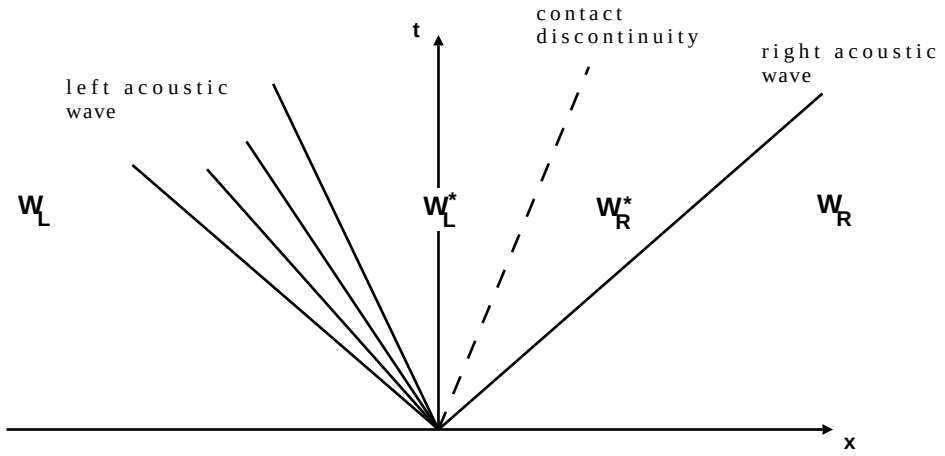

Figure 5.1: Riemann solution showing the intermediate states $\mathbf{W_L}, \mathbf{W_L^*}, \mathbf{W_R^*}, \mathbf{W_R}$.

Note that the solution to a Riemann problem is constant along lines $\frac{x}{t} = constant$. So if we consider a finite-volume formulation with piecewise constant states $\{\mathbf{W}_i\}$, no averaging is required to find the average flux at the interface between the i^{th} and $i^{th}+1$ cells over the course of one time step. The average flux at this interface simply depends on which of the four regions $\mathbf{L}, \mathbf{L}^*, \mathbf{R}^*$ or $\mathbf{R}$, from the Riemann problem $(\mathbf{W}_i, \mathbf{W}_{i+1})$, straddles the time axis. Note that this reasoning assumes that waves emanating from the two neighbouring interfaces do not cross this interface during the course of the time step. That is, the Courant number restriction is satisfied.

Roe[54] has argued that, since the Riemann problems arising from the above method relate only to an approximation of the data, then one might be reasonably satisfied with approximate solutions to these Riemann problems provided that the solutions still describe important non-linear behaviour. The motivation being that these approximate solutions are much cheaper to compute than the exact solutions. Subsequently several approximate Riemann solvers have been developed [21, 45, 64]. The reader is referred to the original papers of Roe[52, 53, 54] and Roe & Pike[58] for an excellent exposition of the development of Roe's scheme for one-dimensional flows.

Now consider a two-dimensional Riemann problem where again we have two semi-infinite states $\mathbf{W_L}$ and $\mathbf{W_R}$, but these states have an additional component of velocity, V, that runs parallel to the specified discontinuity. The solution to this problem will contain the three waves described above plus a shear wave. This wave accounts for any difference in the components of velocity V_L and V_R. Note there is no shear across the other waves. Now, this shear wave is co-incident with the contact discontinuity and so effectively there are still three waves separating four states. Therefore, the solution to this two-dimensional problem may be found by solving the original one-dimensional problem in the normal manner and then simply setting, $V_L^* = V_L$ and $V_R^* = V_R$.

5.2 Roe's Method Extended to Two-Dimensions

Several workers[18, 20, 55] are attempting to develop genuine multi-dimensional characteristic based schemes, but these schemes have not yet matured sufficiently to be used routinely. However, the extension of any upwind scheme developed for one-dimensional flows to that of more than one dimension follows routinely provided one critical assumption is made. Namely, waves can only propagate in directions normal to cell interfaces. This simplification allows us to use the two-dimensional Riemann problem, outlined in the previous section, as the basis for the numerical evolution of two-dimensional flows on quasi-rectangular meshes. Although this method is physically incorrect it has been shown by many workers to give satisfactory results. In this section we shall describe how Roe's method may be extended to solve this two-dimensional Riemann problem.

5.2.1 First-Order Method

The two-dimensional Euler equations may be written in conservative form using cartesian coordinates (x, y),

$$\frac{\partial}{\partial \tau}\begin{pmatrix} \rho \\ \rho V_x \\ \rho V_y \\ E_t \end{pmatrix} + \frac{\partial}{\partial x}\begin{pmatrix} \rho V_x \\ P + \rho V_x^2 \\ \rho V_x V_y \\ (E_t + P)V_x \end{pmatrix} + \frac{\partial}{\partial y}\begin{pmatrix} \rho V_y \\ \rho V_y V_x \\ P + \rho V_y^2 \\ (E_t + P)V_y \end{pmatrix} = 0. \tag{5.2}$$

Now consider an isolated interface which forms part of a two-dimensional mesh, see figure 5.2. If we assume waves can only travel normal to cell interfaces, so that the velocity parallel to the interface is simply convected with the flow, then locally the Euler equations reduce to,

$$\frac{\partial \mathbf{W}}{\partial \tau} + \frac{\partial \mathbf{F}}{\partial n} = 0. \tag{5.3}$$

Where the vectors $\mathbf{W}$ and $\mathbf{F}$ are given by,

$$\mathbf{W} = \begin{pmatrix} \rho \\ \rho V_n \\ \rho V_t \\ E_t \end{pmatrix}; \qquad \mathbf{F} = \begin{pmatrix} \rho V_n \\ \rho V_n^2 + P \\ \rho V_n V_t \\ (E_t + P)V_n \end{pmatrix}. \tag{5.4}$$

If θ is the angle that the normal coordinate direction makes with the x-axis, see figure 5.2, then the local normal and tangential velocity components (V_n, V_t) are related to the cartesian components (V_x, V_y) by,

$$\begin{pmatrix} V_n \\ V_t \end{pmatrix} = \begin{pmatrix} \cos\theta & \sin\theta \\ -\sin\theta & \cos\theta \end{pmatrix} \begin{pmatrix} V_x \\ V_y \end{pmatrix}. \tag{5.5}$$

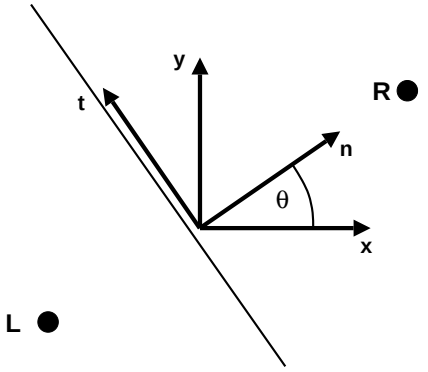

Figure 5.2: Isolated interface which forms part of a two-dimensional mesh.

In essence Roe's scheme replaces the system of equations (5.3) by

$$\frac{\partial \mathbf{W}}{\partial \tau} + \widetilde{\mathbf{A}}(\mathbf{W_L}, \mathbf{W_R}) \frac{\partial \mathbf{W}}{\partial n} = 0. \tag{5.6}$$

Where $\widetilde{\mathbf{A}}(\mathbf{W_L}, \mathbf{W_R})$ is some constant matrix which locally approximates the Jacobian matrix $\frac{\partial \mathbf{F}}{\partial \mathbf{W}}$. The matrix $\widetilde{\mathbf{A}}(\mathbf{W_L}, \mathbf{W_R})$ is constructed to have the following desirable[52] properties:

1. As $\mathbf{W_L} \to \mathbf{W_R} \to \mathbf{W}$, $\quad \widetilde{\mathbf{A}}(\mathbf{W_L}, \mathbf{W_R}) \to \mathbf{A}(\mathbf{W})$, $\quad$ where $\mathbf{A} = \frac{\partial \mathbf{F}}{\partial \mathbf{W}}$.
2. For any $\mathbf{W_L}$,$\mathbf{W_R}$, $\quad \mathbf{F_R} - \mathbf{F_L} = \widetilde{\mathbf{A}}(\mathbf{W_L}, \mathbf{W_R}) \times (\mathbf{W_R} - \mathbf{W_L})$.
3. The eigenvectors of $\widetilde{\mathbf{A}}(\mathbf{W_L}, \mathbf{W_R})$ are linearly independent.

The first property is necessary for the scheme to be consistent. The second property ensures that the scheme is conservative. This enables us to view the eigenvalues of $\widetilde{\mathbf{A}}$ as the wave speeds of a Riemann problem, and the projections of $(\mathbf{W_R} - \mathbf{W_L})$ onto

its eigenvectors as the jumps between the intermediate states $\mathbf{W_L}$,$\mathbf{W_L^*}$,$\mathbf{W_R^*}$ and $\mathbf{W_R}$. While property #3 together with #2 are necessary for the scheme to *recognize* a shock wave. Indeed if the solution to the Riemann problem is a single shock wave then Roe's approximate solver will give the exact solution.

Let the eigenvectors of $\widetilde{\mathbf{A}}(\mathbf{W_L}, \mathbf{W_R})$ be denoted by $\tilde{\mathbf{e}}_k$ and the corresponding eigenvalues by $\tilde{\lambda}_k$ then, by construction we have

$$\mathbf{W_R} - \mathbf{W_L} = \sum_k \alpha_k \tilde{\mathbf{e}}_k \tag{5.7}$$

$$\mathbf{F_R} - \mathbf{F_L} = \sum_k \alpha_k \tilde{\lambda}_k \tilde{\mathbf{e}}_k. \tag{5.8}$$

Each term in the above summations represents the effect of one wave, α_k is the strength of the k^{th} wave, and $\tilde{\lambda}_k$ is its speed. Now the flux at an interface $i+\frac{1}{2}$ separating two states $\mathbf{W_L}, \mathbf{W_R}$ could be computed from either

$$\mathbf{F}_{i+\frac{1}{2}}(\mathbf{W_L}, \mathbf{W_R}) = \mathbf{F_L} + \sum\nolimits^{(-)} \alpha_k \tilde{\lambda} \tilde{\mathbf{e}}_k \tag{5.9}$$

or

$$\mathbf{F}_{i+\frac{1}{2}}(\mathbf{W_L}, \mathbf{W_R}) = \mathbf{F_R} - \sum\nolimits^{(+)} \alpha_k \tilde{\lambda} \tilde{\mathbf{e}}_k, \tag{5.10}$$

where $\sum^{(-)}$ and $\sum^{(+)}$ denote summations over negative and positive wave speeds respectively. We can take the average of these two expressions to get,

$$\mathbf{F}_{i+\frac{1}{2}}(\mathbf{W_L}, \mathbf{W_R}) = \frac{1}{2}(\mathbf{F_L} + \mathbf{F_R}) - \frac{1}{2}\sum_k \alpha_k \left|\tilde{\lambda}_k\right| \tilde{\mathbf{e}}_k. \tag{5.11}$$

This is equivalent to setting $\mathbf{F}_{i+\frac{1}{2}}$ equal to whichever of the four flux states $\mathbf{F_L}$,$\mathbf{F_L^*}$,$\mathbf{F_R^*}$ or $\mathbf{F_R}$ from the Riemann problem $(\mathbf{W_L}, \mathbf{W_R})$ straddles the interface, see figure 5.1. Note that if we have four waves numbered 1,2,3,4 from left to right then,

$$\begin{aligned} \mathbf{F_L^*} &= \mathbf{F_L} + \alpha_1 \tilde{\lambda}_1 \tilde{\mathbf{e}}_1 \\ \mathbf{F_R^*} &= \mathbf{F_R} - \alpha_4 \tilde{\lambda}_4 \tilde{\mathbf{e}}_4. \end{aligned} \tag{5.12}$$

The form of the jacobian matrix $\widetilde{\mathbf{A}}$ for the system of equations (5.3) is easily found,

$$\widetilde{\mathbf{A}} = \begin{pmatrix} 0 & 1 & 0 & 0 \\ (\gamma-1)\frac{q^2}{2} - \tilde{V}_n^2 & (3-\gamma)\tilde{V}_n & (1-\gamma)\tilde{V}_t & (\gamma-1) \\ -\tilde{V}_n\tilde{V}_t & \tilde{V}_t & \tilde{V}_n & 0 \\ \tilde{V}_n\left[(\gamma-1)q^2 - \frac{\gamma\tilde{E}_t}{\tilde{\rho}}\right] & \frac{\gamma\tilde{E}_t}{\tilde{\rho}} + (1-\gamma)\left[\frac{q^2}{2} + \tilde{V}_n^2\right] & (1-\gamma)\tilde{V}_n\tilde{V}_t & \gamma\tilde{V}_n \end{pmatrix}, \tag{5.13}$$

where,

$$q^2 = \tilde{V}_n^2 + \tilde{V}_t^2. \tag{5.14}$$

The eigenvectors and corresponding eigenvalues of this matrix are,

$$\tilde{\mathbf{e}}_1 = \begin{pmatrix} 1 \\ \tilde{V}_n - \tilde{a} \\ \tilde{V}_t \\ \tilde{H} - \tilde{a} \end{pmatrix}; \quad \tilde{\mathbf{e}}_2 = \begin{pmatrix} 1 \\ \tilde{V}_n \\ \tilde{V}_t \\ \frac{1}{2}\left[\tilde{V}_n^2 + \tilde{V}_t^2\right] \end{pmatrix}; \quad \tilde{\mathbf{e}}_3 = \begin{pmatrix} 0 \\ 0 \\ 1 \\ \tilde{V}_t \end{pmatrix}; \quad \tilde{\mathbf{e}}_4 = \begin{pmatrix} 1 \\ \tilde{V}_n + \tilde{a} \\ \tilde{V}_t \\ \tilde{H} + \tilde{a} \end{pmatrix}. \tag{5.15}$$

$$\tilde{\lambda}_1 = \tilde{V}_n - \tilde{a}; \qquad \tilde{\lambda}_2 = \tilde{V}_n; \qquad \tilde{\lambda}_3 = \tilde{V}_n; \qquad \tilde{\lambda}_4 = \tilde{V}_n + \tilde{a}. \tag{5.16}$$

Where,

$$\tilde{a}^2 = (\gamma - 1)\left[\tilde{H} - \frac{1}{2}\left(\tilde{V}_n^2 + \tilde{V}_t^2\right)\right]. \tag{5.17}$$

Waves #1 and #4 can each represent either a shock or an expansion wave. Wave #2 represents a contact discontinuity and wave #3 a shear wave. We may substitute for $\{\tilde{\mathbf{e}}_k\}$ and $\left\{\tilde{\lambda}_k\right\}$ into equation (5.7), this will give four simultaneous equations which we may then solve to find the wave strengths $\{\alpha_k\}$. These are

$$\begin{aligned} \alpha_1 &= \tfrac{\Delta P - \tilde{\rho}\tilde{a}\Delta V_n}{2\tilde{a}^2} & \alpha_2 &= \Delta\rho - \tfrac{\Delta P}{\tilde{a}^2} \\ \alpha_3 &= \tilde{\rho}\Delta V_t & \alpha_4 &= \tfrac{\Delta P + \tilde{\rho}\tilde{a}\Delta V_n}{2\tilde{a}^2} \end{aligned} \tag{5.18}$$

with,

$$\Delta() = ()_R - ()_L. \tag{5.19}$$

It was shown by Roe & Pike[58] that the only form of averaging $\widetilde{()}$ that satisfies equation (5.8) exactly is,

$$\begin{aligned} \tilde{\rho} &= \sqrt{\rho_L \rho_R} \\ \tilde{V}_n &= \frac{\sqrt{\rho_L}V_{n_L} + \sqrt{\rho_R}V_{n_R}}{\sqrt{\rho_L} + \sqrt{\rho_R}} \\ \tilde{V}_t &= \frac{\sqrt{\rho_L}V_{t_L} + \sqrt{\rho_R}V_{t_R}}{\sqrt{\rho_L} + \sqrt{\rho_R}} \\ \tilde{H} &= \frac{\sqrt{\rho_L}H_L + \sqrt{\rho_R}H_R}{\sqrt{\rho_L} + \sqrt{\rho_R}}. \end{aligned} \tag{5.20}$$

The original analysis was done for one-dimensional flows and so did not include $\tilde{V}_t$, but it may be shown that $\tilde{V}_t$ must also be averaged in this manner.

Equation (5.11) and equations (5.15) to (5.20) constitute Roe's approximate Riemann solver.

5.2.2 Second-Order Extension

For practical purposes the first-order method outlined above proves to be too diffusive, and a second-order method is required. We shall now state the second-order extension developed by Roe[54] and demonstrate that this scheme reduces to Lax-Wendroff in smooth regions of the flow.

The second-order analogue to the first-order flux given in equation (5.11) is,

$$\mathbf{F}_{i+\frac{1}{2}}(\mathbf{W_L}, \mathbf{W_R}) = \frac{1}{2}(\mathbf{F_L} + \mathbf{F_R}) - \frac{1}{2}\sum_k \alpha_k \left[1 - B_k\left(1 - |\nu_k|\right)\right]\left|\tilde{\lambda}_k\right|\tilde{\mathbf{e}}_k. \tag{5.21}$$

Where ν_k is the Courant number of the k^{th} wave and B_k is a non-linear limiter function. A description of the form taken by these limiter functions will be given in the next section. Here we simply note the following. In non-smooth regions of the flow $B_k \rightarrow 0$ and this second-order flux reduces to the first-order flux. Therefore the second-order scheme will have the monotonicity preserving characteristics of the first-order scheme. While in smooth regions of the flow $B_k \rightarrow 1$ and the scheme has the second-order accuracy associated with the Lax-Wendroff scheme. This is easily shown for the linear advection equation,

$$\frac{\partial u}{\partial t} + a\frac{\partial u}{\partial x} = 0. \tag{5.22}$$

This equation may be discretized as,

$$u^{n+1} = u^n - \frac{\Delta t}{\Delta x}\left(f^{n+\frac{1}{2}}_{i+\frac{1}{2}} - f^{n+\frac{1}{2}}_{i-\frac{1}{2}}\right), \tag{5.23}$$

where $f^n_i = a u^n_i$. Now if $B_k = 1$ the interface flux given by equation (5.21) will reduce to,

$$f^{n+\frac{1}{2}}_{i+\frac{1}{2}} = \frac{a}{2}\left(u^n_i + u^n_{i+1}\right) - \frac{\nu a}{2}\left(u^n_{i+1} - u^n_i\right). \tag{5.24}$$

This allows us to re-write equation (5.23) in the form,

$$u^{n+1}_i = \frac{\nu\left(1+\nu\right)}{2}u^n_{i-1} + \left(1-\nu^2\right)u^n_i - \frac{\nu\left(1-\nu\right)}{2}u^n_{i+1}, \tag{5.25}$$

which may be recognised as one form of the Lax-Wendroff scheme.

The flux given in equation (5.21) is suitable for a mesh integrator that uses operator splitting. The form of the interface flux suggested by Roe[56] for finite-volume formulations differs slightly,

$$\mathbf{F}_{i+\frac{1}{2}}(\mathbf{W_L}, \mathbf{W_R}) = \frac{1}{2}\left(\mathbf{F_L} + \mathbf{F_R}\right) - \frac{1}{2}\sum_k \alpha_k \left[1 - B_k\right]\left|\tilde{\lambda}_k\right|\tilde{\mathbf{e}}_k. \tag{5.26}$$

In smooth regions of the flow this formulation reduces to central differencing. A stable scheme is produced by combining this flux formulation with a Runge-Kutta time integration scheme, this form of the interface flux is similar to that used by Jameson[33], except here the artificial viscosity dissipation has been replaced by an *intelligent* upwind dissipation.

The flux formulations given above are only formally second-order accurate for uniformly spaced meshes but do retain their accuracy on smoothly varying meshes. Pike[46] has examined the modifications that must be made to Roe's method so as to ensure that the scheme remains formally second-order accurate on irregularly spaced meshes, but we do not consider this extension here.

5.2.3 Limiter Functions

Godunov's theorem states that no second- or higher-order accurate numerical scheme for the linear advection equation can preserve monotonicity if its computational stencil has constant coefficients. It was long thought that this theorem excluded the possibility of computing second-order accurate solutions to the Euler equations that would exhibit monotonic shock profiles. Van Leer[66] realised that monotone solutions could be computed but that the marching algorithm must be non-linear, even when applied to linear problems. Several authors have developed non-linear algorithms that have certain specified properties for the linear advection equation. These algorithms are then empirically extended to the Euler equations. In general, at least for the linear advection equation, these different schemes are more or less equivalent. Underpinning these non-linear algorithms is the concept of limiter functions[53]. A full description of these limiter functions is beyond the scope of this work. But we give formulae for two limiter functions that are commonly employed with Roe's method.

$$\begin{aligned} MinMod(r_k) &= max(0, min(1, r_k)) \\ SuperBee(r_k) &= max(0, min(1, 2r_k), min(2, r_k)) \end{aligned} \tag{5.27}$$

A suitable choice for the parameter r_k is the ratio of the upwind to local wave strengths,

$$r_k = \frac{(\alpha_k)_{upwind}}{(\alpha_k)_{local}}, \tag{5.28}$$

this allows each wave of the approximate Riemann solution to be limited separately. Note in smooth regions of the flow $r_k \to 1$ and $B(r_k) \to 1$, while near extrema, $r_k < 0$ and so $B(r_k) = 0$.

5.3 Known Problems with Roe's Method

Today's modern high resolution shock capturing schemes are robust and give reliable results for a wide range of problems without needing to be retuned. This represents a major advance upon artificial viscosity methods. However, even these modern schemes are far from perfect, many of them are known to fail under certain conditions. Details are now given about the conditions for which Roe's method is known to fail, and for the *fixes* that are commonly employed to prevent these failures.

5.3.1 Entropy Condition

It is well known that the basic version of Roe's scheme does not satisfy an *entropy condition*[53], that is the scheme can admit non-physical solutions such as expansion shocks. This problem does not just afflict Roe's method. Osher[44] has found a general condition

for a scheme to be entropy satisfying when applied to scalar equations, he designates such schemes E-schemes. However, at present any extension to a system of equations contains a large amount of empiricism and must therefore remain suspect. Indeed, Godunov's method is classified as an E-scheme but can still give rise to nearly discontinuous expansion fans near sonic points. Several *fixes* exist in the literature that prevent Roe's method from admitting expansion shocks, we shall now describe two of them.

Harten[74] has noted that the entropy violation inherent in Roe's scheme is related to the fact that the numerical viscosity vanishes for $\nu = 0$. His solution is to replace values of ν smaller than some tolerance δ with larger values ν',

$$\begin{cases} \nu' = \frac{\nu}{2}\left[\frac{\nu^2}{\delta} + \delta\right] & \text{for} \quad |\nu| < 2\delta \\ \nu' = \nu & \text{for} \quad |\nu| \geq 2\delta. \end{cases} \tag{5.29}$$

This modification to the wave speeds is only applied to the acoustic waves, the contact and shear waves are linearly degenerate and do not violate the entropy condition. He notes that the dependence on δ is slight but that a larger value of δ improves the enforcement of the entropy condition at the expense of a slight loss in resolution of the scheme. Typically δ is set to 0.1. Although Harten's *entropy fix* works quite well, two objections can be made against it. First, a tunable parameter δ has been introduced into the scheme. Second, there seems to be little physical justification for its use. Both these points suggest that the *fix* is at odds with the thesis adopted by Roe for the development of the basic scheme.

Roe[53] has devised an *entropy fix* based on estimates for the spreading rate δ_k of each wave within the approximate Riemann solution. Now neither compression waves, contact discontinuities nor shear waves spread and so δ_k for these waves is zero. Across simple expansion fans the Riemann invariant does not change,

$$a + \frac{(\gamma - 1)}{2} V_n = \text{constant}. \tag{5.30}$$

Therefore, if the left acoustic wave is an expansion then an estimate for the velocity difference between the characteristics bounding the fan is given by,

$$\delta_1 = \Delta^{(1)}(V_n - a) = \frac{\gamma + 1}{2}\Delta^{(1)} V_n. \tag{5.31}$$

Similarly, if the right acoustic wave is an expansion then,

$$\delta_4 = \Delta^{(4)}(V_n + a) = \frac{\gamma + 1}{2}\Delta^{(4)} V_n. \tag{5.32}$$

The changes in the normal component of velocity across these two acoustic waves may be estimated from,

$$\begin{aligned} \Delta^{(1)} V_n &= -\frac{\alpha_1 \tilde{a}}{\tilde{\rho}} \\ \Delta^{(4)} V_n &= +\frac{\alpha_4 \tilde{a}}{\tilde{\rho}}. \end{aligned} \tag{5.33}$$

Corrective action need only be taken if the spreading rate for the k^{th} wave is greater than twice the modulus of the mean wave speed, that is $\delta_k > 2\left|\tilde{\lambda}_k\right|$. Because then the leftmost and rightmost characteristics in the expansion fan are moving in opposite directions, see figure 5.3. In such cases we split the wave up into two characteristics left and right with speeds $\tilde{\lambda}_k - \frac{\delta_k}{2}$ and $\tilde{\lambda} + \frac{\delta_k}{2}$ respectively. We assign half the original wave strength α_k to these two new waves, this ensures that the combined flux jump across the two waves is the same as that across the original single mean wave,

$$\alpha_k \tilde{\lambda}_k \tilde{\mathbf{e}}_k = \frac{\alpha_k}{2}\left(\tilde{\lambda}_k - \frac{\delta_k}{2}\right)\tilde{\mathbf{e}}_k + \frac{\alpha_k}{2}\left(\tilde{\lambda}_k + \frac{\delta_k}{2}\right)\tilde{\mathbf{e}}_k. \tag{5.34}$$

This mechanism provides sufficient spreading of expansion fans to avoid the formation of expansion shocks. We may therefore re-formulate the first-order interface flux given in equation (5.11) as,

$$\mathbf{F}_{i+\frac{1}{2}}(\mathbf{W_L}, \mathbf{W_R}) = \frac{1}{2}(\mathbf{F_L} + \mathbf{F_R}) - \frac{1}{2}\sum_k \alpha_k \left[\left|\tilde{\lambda}_k - \frac{\delta_k}{2}\right| + \left|\tilde{\lambda}_k + \frac{\delta_k}{2}\right|\right]\tilde{\mathbf{e}}_k. \tag{5.35}$$

The two *entropy fixes* outlined above are both successful in that they prevent Roe's scheme from admitting expansion shocks, but their accuracy remains questionable. The correct formulation for sonic fluxes remains an active research area, recent papers on the subject include Roe[57].

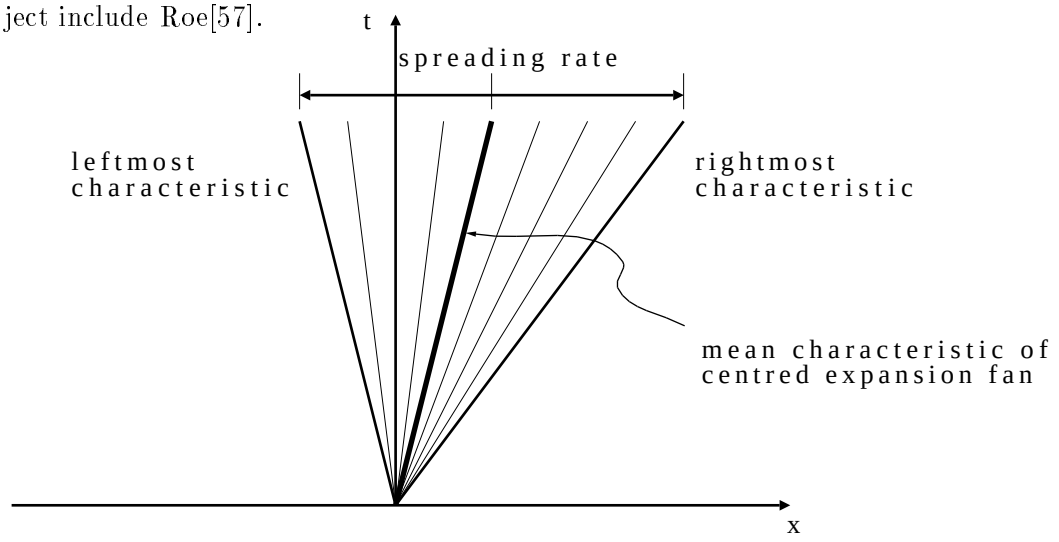

Figure 5.3: Roe's *entropy fix*.

5.3.2 Positivity

It has been observed that for highly energetic flows, a numerical approximation to the conservation laws of mass and momentum can, for certain parts of the flowfield, result in the kinetic energy of the fluid being greater than the total energy which is found

by the numerical approximation to the conservation law of energy. This implies that the internal energy of the fluid is negative, which in turn implies that the pressure is negative. Obviously this behaviour is non-physical. Therefore, a pre-requisite for any numerical scheme to successfully model highly energetic flows must be the property that the internal energy and density of the fluid remain positive throughout the calculation, such schemes are termed *positively conservative* [22]. Godunov's scheme is *positively conservative*, whereas any Godunov-type scheme based on a linearized Riemann solution is not. Einfeldt[21] has argued that these linearized methods fail because the numerical signal speeds under-estimate the physical signal speeds within the Riemann solution; the greater the signal speed, the greater the numerical dissipation and the better the behaviour of the scheme near low densities.

Roe's method can be made *positively conservative* by replacing the standard wave speeds $\left\{\tilde{\lambda}_k\right\}$ by,

$$\begin{aligned}
\tilde{\lambda}'_1 &= \frac{b^{(+)}+b^{(-)}}{b^{(+)}-b^{(-)}}.\tilde{\lambda}_1 - 2\frac{b^{(+)}b^{(-)}}{b^{(+)}-b^{(-)}} \qquad (5.36)\\
\tilde{\lambda}'_2 &= \frac{b^{(+)}+b^{(-)}}{b^{(+)}-b^{(-)}}.\tilde{\lambda}_2 - 2\frac{b^{(+)}b^{(-)}}{b^{(+)}-b^{(-)}}(1-\delta)\\
\tilde{\lambda}'_3 &= \frac{b^{(+)}+b^{(-)}}{b^{(+)}-b^{(-)}}.\tilde{\lambda}_3 - 2\frac{b^{(+)}b^{(-)}}{b^{(+)}-b^{(-)}}(1-\delta)\\
\tilde{\lambda}'_4 &= \frac{b^{(+)}+b^{(-)}}{b^{(+)}-b^{(-)}}.\tilde{\lambda}_4 - 2\frac{b^{(+)}b^{(-)}}{b^{(+)}-b^{(-)}}.
\end{aligned}$$

Where,

$$\begin{aligned}
b^{(+)} &= max(\tilde{\lambda}_4, V_{n_R}+a_R, 0) \qquad (5.37)\\
b^{(-)} &= min(\tilde{\lambda}_1, V_{n_L}-a_L, 0)
\end{aligned}$$

and,

$$\delta = \frac{\tilde{a}}{\tilde{a}+\frac{1}{2}|max(\tilde{\lambda}_4, V_{n_R}+a_R)+min(\tilde{\lambda}_1, V_{n_L}-a_L)|}. \qquad (5.38)$$

Full details of this modification may be found in[21, 22]. This *fix* also makes Roe's scheme *entropy satisfying*, however, it should be noted that this modification to the wave speeds is only valid for the first-order method.

5.3.3 Shear Waves

Recently we have made observations that suggest Roe's method can admit spurious solutions that are triggered by an incorrect treatment of shear waves. Hitherto this mode of failure has not been reported in the literature and so we present our observations in full.

Figures 5.4 and 5.5 show the results, density contours drawn at 2.5% intervals, of computing the reflection of a plane shock, $M_s = 5.5$ and $\gamma = 1.4$, from a 30^o wedge with interface fluxes calculated using first-order versions of Roe's approximate Riemann solver and an exact Riemann solver respectively. The solution to this type of problem is well documented[28], and for our specific case we expect a type of solution known as double Mach reflection (DMR). These first-order results are too diffusive to resolve the complicated flow structure behind the Mach stem. Nevertheless, one would still expect the Mach stem to remain roughly perpendicular to the surface of the wedge. This is true for the calculation done with the exact Riemann solver, but the Mach stem obtained with the approximate solver is severely kinked. Initially we suspected that there was a bug in our implementation of Roe's method. But this seemed unlikely for, in every other respect the results from these two calculations are very similar. Furthermore, the single Mach reflection calculation presented in §4.4.2 used the same computational grid and the same computer code as we have used here, but for this SMR problem the Mach stem remained normal to the surface of the wedge! So we abandoned our search for a coding error and concluded that the approximate solver is failing in some sense. Subsequently we have learnt that other workers [15] have made similar observations, this would seem to confirm our conclusion, but they offer no satisfactory explanations as to why the kinking occurs.

Now, we cannot as yet explain the exact mechanism by which the approximate solver fails. However, a comparison of the form of solution given by Roe's approximate solver with that of the exact solution clearly illustrates that a shear velocity can induce fundamental differences between the two solutions. Consider the general solution to the Riemann problem $(\mathbf{W_L}, \mathbf{W_R})$ shown in figure 5.1. Now suppose that the prescribed tangential component of velocity V_{t_R} is replaced by $-V_{t_R}$ and call this new right-hand state $\mathbf{W'_R}$. The exact solution to this new Riemann problem $(\mathbf{W_L}, \mathbf{W'_R})$ is the same as before except that $V^*_{t_R} = V'_{t_R} = -V_{t_R}$. However, for Roe's approximate solver the form of solution to these two problems will be very different. This is an inevitable consequence of the linearization process. For, the average value $\tilde{V}_t$ must be different and therefore the acoustic wave speeds and wave strengths must also differ. Now if a change in the prescribed shear velocity can result in a difference between the approximate solutions that is not present between the exact solutions, then the approximate solver could be lacking some desirable property inherent in the exact solver. The absence of this property may be responsible for the behaviour exhibited in figure 5.4.

Additionally, a close inspection of Roe's method reveals that shear can be introduced across the acoustic waves. Again this deviation from the exact solution is directly attributable to the linearization process. The changes in density and the shear component of momentum across the left acoustic wave are given by,

$$\begin{aligned} \Delta\rho &= \alpha_1 \\ \Delta(\rho V_t) &= \alpha_1 \tilde{V}_t = \tilde{V}_t \Delta\rho. \end{aligned} \tag{5.39}$$

Therefore the effective value of V_t within the region $\mathbf{W_L^*}$ may be found.

$$V_{t_L}^* = \frac{\rho_L V_{t_L} + \tilde{V}_t \Delta\rho}{\rho_L + \Delta\rho} = V_{t_L} + (\tilde{V}_t - V_{t_L})\frac{\Delta\rho}{\rho_L + \Delta\rho}. \tag{5.40}$$

From which it can be seen that $V_{t_L}^*$ only has the correct value, V_L, if $\Delta\rho = 0$ or if no shear is present, that is $\tilde{V}_t = V_{t_L} = V_{t_R}$. A similar argument holds for the right acoustic wave.

Further work needs to be done to try and isolate the mechanism of failure exhibited in figure 5.4, however, a re-formulation of Roe's method based upon physical arguments has shown promising results in eliminating this problem.

5.4 Roe's Method Re-Formulated

It is becoming increasingly apparent that no one Riemann solver, exact or approximate is going to be better than all other solvers for all problems. For example, Roe's approximate solver while reasonably efficient computationally suffers from the problems outlined above. Some other approximate solvers do not suffer from these problems but give inadequate resolution, especially of contact discontinuities. While exact Riemann solvers are often computationally too expensive. So an increasingly vexing question is, what Riemann solver should one use in practice? A possible answer to this conundrum might be, don't use any one Riemann solver, but instead use several solvers. One could employ a hierarchical set of Riemann solvers. At the bottom of the hierarchy would be computationally cheap, but low resolution schemes. These schemes would be used in those regions where the flow activity is small, often this proves to be most of the flowfield. While progressively higher resolution schemes could be used the greater the flow activity. This concept of matching the resolution of the Riemann solver to the local flow conditions would seem to be a natural progression from the concepts of adaptively refining the mesh in regions of interest.

Leaving aside the problem of how to choose which Riemann solver should be applied to a given interface, there exists one major obstacle to the practicability of such a scheme. Namely, how to formulate these different Riemann solvers such that the same basic machinery may be employed to arrive at a second-order scheme. The easiest way to achieve this goal would be to adopt a MUSCL[67] approach. For such schemes, second-order accuracy is achieved by a pre-processing of the data supplied to the Riemann solver rather than by a direct modification to the Riemann solver. However, the resolution achieved by this geometric approach is generally inferior to that achieved by methods that post-process the Riemann solution, that is flux limited methods. Because the post-processing method allows the limiting to be done on a wave by wave basis, whereas the geometric pre-processing is analogous to limiting all the waves by an amount set by the worst case wave. We shall now describe a method of flux limiting that is suitable for most Riemann

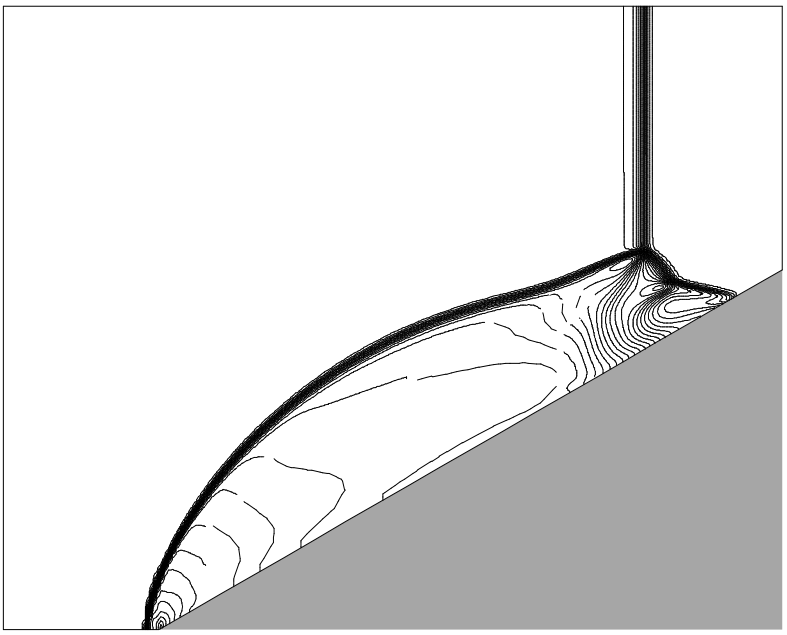

Figure 5.4: DMR; Standard Roe scheme, first-order.

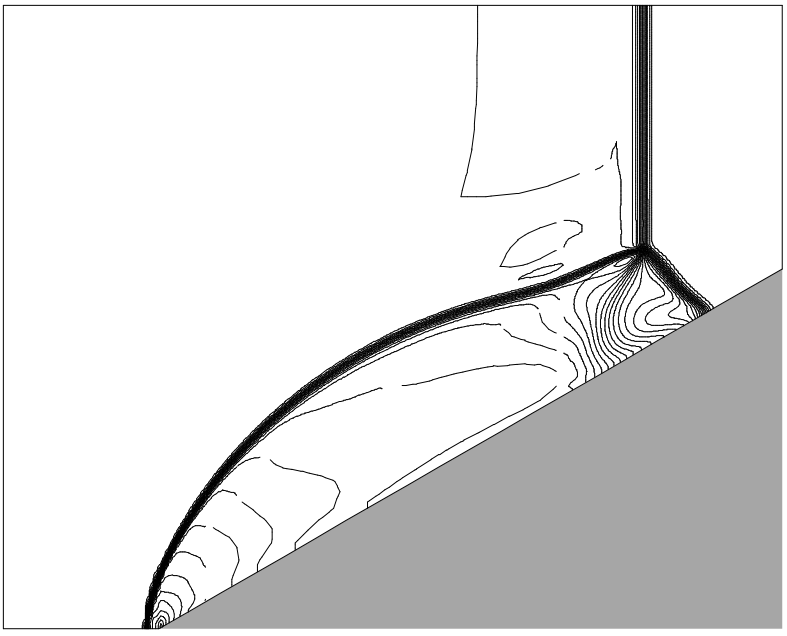

Figure 5.5: DMR; Exact Riemann solver, first-order.

solvers whether approximate or exact. The method will be developed by analogy with Roe's second-order scheme.

5.4.1 Weighted Average Flux Formulation

The flux formulation given in equation (5.21) may be re-interpreted as the Weighted Average Flux, WAF, proposed by Toro[64]. This equation may be re-written as,

$$\mathbf{F}_{i+\frac{1}{2}}(\mathbf{W_L},\mathbf{W_R}) = \frac{1}{2}\left(\mathbf{F_L}+\mathbf{F_R}\right) - \frac{1}{2}\sum_k \alpha_k \frac{\left[1-B_k\left(1-|\nu_k|\right)\right]}{|\nu_k|}\nu_k\tilde{\lambda}_k\tilde{\mathbf{e}}_k. \tag{5.41}$$

We choose to re-write this as,

$$\mathbf{F}_{i+\frac{1}{2}}(\mathbf{W_L},\mathbf{W_R}) = \frac{1}{2}\left(\mathbf{F_L}+\mathbf{F_R}\right) - \frac{1}{2}\sum_k \nu'_k\alpha_k\tilde{\lambda}_k\tilde{\mathbf{e}}_k, \tag{5.42}$$

where,

$$\nu'_k = \frac{\left[1-B_k\left(1-|\nu_k|\right)\right]}{|\nu_k|}\nu_k. \tag{5.43}$$

Now we can relate the wave flux jumps $\alpha_k\tilde{\lambda}_k\tilde{\mathbf{e}}_k$ to the differences between the fluxes $\mathbf{F_L}, \mathbf{F^*_L}, \mathbf{F^*_R}$ and $\mathbf{F_R}$ as follows,

$$\begin{aligned}
\mathbf{F^*_L}-\mathbf{F_L} &= \alpha_1\tilde{\lambda}_1\tilde{\mathbf{e}}_1 \\
\mathbf{F^*_R}-\mathbf{F^*_L} &= \alpha_2\tilde{\lambda}_2\tilde{\mathbf{e}}_2+\alpha_3\tilde{\lambda}_3\tilde{\mathbf{e}}_3 \\
\mathbf{F^*_R}-\mathbf{F_R} &= \alpha_4\tilde{\lambda}_4\tilde{\mathbf{e}}_4.
\end{aligned} \tag{5.44}$$

This enables us to expand equation (5.41) to give,

$$\mathbf{F}_{i+\frac{1}{2}}(\mathbf{W_L},\mathbf{W_R}) = \frac{1}{2}\left(\mathbf{F_L}+\mathbf{F_R}\right) - \frac{\nu'_L}{2}\left[\mathbf{F^*_L}-\mathbf{F_L}\right] - \frac{\nu'_*}{2}\left[\mathbf{F^*_R}-\mathbf{F^*_L}\right] - \frac{\nu'_R}{2}\left[\mathbf{F_R}-\mathbf{F^*_R}\right]. \tag{5.45}$$

Where we have replaced ν'_1 by ν'_L, $\nu'_{2,3}$ by ν_* and ν'_4 by ν'_R, see figure 5.6. This equation can be rearranged to give,

$$\mathbf{F}_{i+\frac{1}{2}}(\mathbf{W_L},\mathbf{W_R}) = w_1\mathbf{F_L} + w_2\mathbf{F^*_L} + w_3\mathbf{F^*_R} + w_4\mathbf{F_R} \tag{5.46}$$

with,

$$\begin{aligned}
w_1 &= \frac{1+\nu'_L}{2} \\
w_2 &= \frac{\nu'_*-\nu'_L}{2} \\
w_3 &= \frac{\nu'_R-\nu'_*}{2} \\
w_4 &= \frac{1-\nu'_R}{2}.
\end{aligned} \tag{5.47}$$

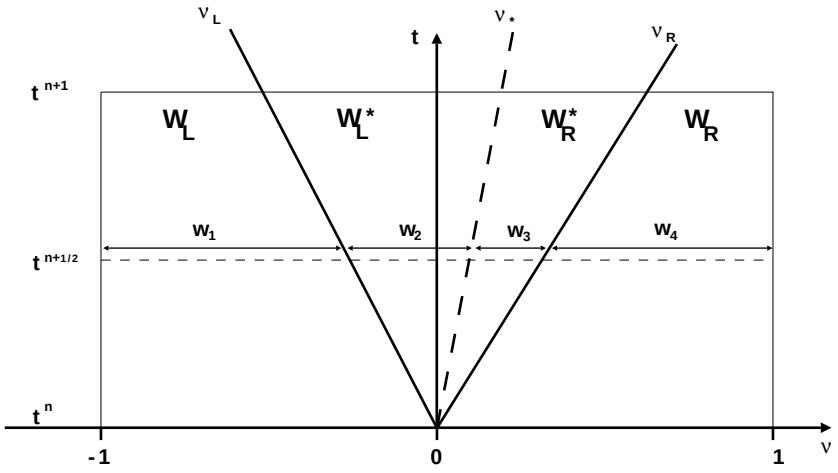

Figure 5.6: Weights given by a Riemann solution at time $t^{n+\frac{1}{2}}$.

This expression is equivalent to the WAF formulation given by Toro for,

$$\nu_k' = \frac{[1 - B_k\,(1 - |\nu_k|)]}{|\nu_k|}\nu_k = A_k\nu_k. \tag{5.48}$$

Where A_k, using WAF terminology, is called an amplification factor. The WAF formulation enables us to construct a second-order interface flux from any Riemann-type solver that can provide the fluxes $\mathbf{F_L^*}, \mathbf{F_R^*}$ and the wave speeds $\lambda_L, \lambda_*, \lambda_R$. For example, for Roe's approximate solver we simply have,

$$\begin{aligned} \mathbf{F_L^*} &= \mathbf{F_L} + \alpha_1\tilde{\lambda}_1\tilde{\mathbf{e}}_1 \\ \mathbf{F_R^*} &= \mathbf{F_R} + \alpha_4\tilde{\lambda}_4\tilde{\mathbf{e}}_4, \end{aligned} \tag{5.49}$$

note we now only have to compute two of the four flux jumps. While for an exact Riemann solver we have,

$$\begin{aligned} \mathbf{F_L^*} &= \mathbf{F}(\mathbf{W_L^*}) \\ \mathbf{F_R^*} &= \mathbf{F}(\mathbf{W_R^*}). \end{aligned} \tag{5.50}$$

Moreover, by analogy with Roe's method we can employ a single method to calculate the amplification factors A_k. Consider the amplification factor given in equation (5.48). It is a function of the wave speed and the ratio of the upwind to local wave strengths. But these wave strengths are equal to the density jumps across waves. Therefore, if for an exact Riemann solver we construct the pseudo wave strengths $\rho_R - \rho_R^*, \rho_R^* - \rho_L^*, \rho_L^* - \rho_L$ we may then use the same machinery as was used by Roe's method to calculate these amplification factors. This method has been applied to an exact Riemann solver and works well, figure 5.7 shows results for the shock reflection problem outlined above. The amplification factor was calculated using the MINMOD limiter function.

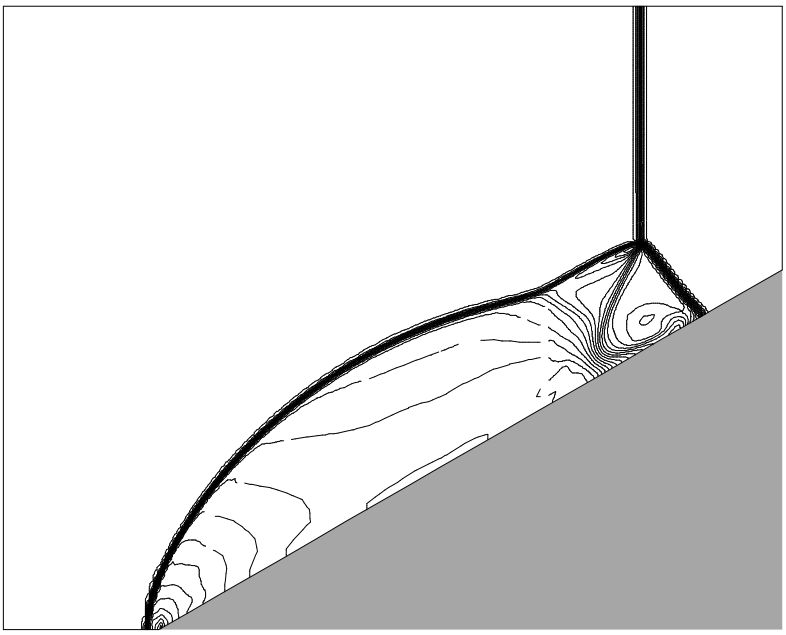

Figure 5.7: DMR; WAF using an exact Riemann solver and MINMOD limiter.

5.4.2 A *Shear Fix* for Roe's Method

The motivation for re-formulating Roe's scheme as a WAF method was so that it would be more convenient to incorporate the scheme into a hierarchical Riemann solver. However, the WAF formulation also allows us to develop a possible *fix* to the shear problem outlined above. We shall develop this *fix* more by physical argument than by rigorous mathematical analysis.

First, we note that simply changing the sign of one of the two shear components of velocity that are prescribed for the Riemann problem $(\mathbf{W_L}, \mathbf{W_R})$ does not significantly alter the exact solution. Indeed the wave speeds do not change at all. But for Roe's scheme the average sound speed is calculated using,

$$\tilde{a}^2 = (\gamma - 1)\left[\tilde{H} - \frac{1}{2}(\tilde{V}_n^2 + \tilde{V}_t^2)\right]. \tag{5.51}$$

This change in sign will alter $\tilde{V}_t$ which in turn will alter $\tilde{a}$. We therefore propose that this equation for $\tilde{a}$ be replaced by,

$$\tilde{a}^2 = (\gamma - 1)\left[\tilde{H} - \frac{1}{2}(\tilde{V}_n^2 + \widetilde{V_t^2})\right]. \tag{5.52}$$

Second, we have shown that shear can be introduced across the two acoustic waves. We can enforce the correct physical behaviour, namely V_t does not change across these waves,

by arbitrarily replacing $\tilde{V}_t$ by V_L for $\tilde{\mathbf{e}}_1$ and by V_R for $\tilde{\mathbf{e}}_4$. These two eigenvectors are now given by,

$$\tilde{\mathbf{e}}_1 = \begin{pmatrix} 1 \\ \tilde{V}_n - \tilde{a} \\ V_{t_L} \\ \left[\frac{\tilde{a}^2}{(\gamma-1)} + \frac{1}{2}(\tilde{V}_n^2 + V_{t_L}^2)\right] - a\tilde{V}_n \end{pmatrix}; \quad \tilde{\mathbf{e}}_4 = \begin{pmatrix} 1 \\ \tilde{V}_n + \tilde{a} \\ V_{t_R} \\ \left[\frac{\tilde{a}^2}{(\gamma-1)} + \frac{1}{2}(\tilde{V}_n^2 + V_{t_R}^2)\right] + a\tilde{V}_n \end{pmatrix}. \tag{5.53}$$

Note for the WAF formulation we do not need to compute $\tilde{\mathbf{e}}_2$ and $\tilde{\mathbf{e}}_3$.

These two simple modifications are sufficient to ensure that the approximate Riemann solver gives results, at least for the shock reflection problem, that are comparable to those given by the exact Riemann solver, compare figures 5.7 & 5.8. The difference between these results and those given by the standard scheme is quite marked, see figure 5.9. It should be noted that, if no shear is present then the modified scheme reduces to the original scheme. Therefore, the modified scheme will still *recognize* a shock wave. Moreover, because we have formulated the scheme in terms of fluxes rather than flux differences we have gained the latitude to make the above changes to the evaluation of $\tilde{\mathbf{e}}_1, \tilde{\mathbf{e}}_4$ and $\tilde{a}$. For the flux-difference formulation these modifications would violate one of the essential conditions for the wave decomposition to represent a Riemann solution, namely, that the sum for all waves of the flux jumps across each wave should be equal to the flux difference $\mathbf{F_R} - \mathbf{F_L}$.

We end this section by noting that it is possible to effect a similar *shear fix* for the standard flux-difference split scheme by applying Harten's *entropy fix* , with a suitably large value of δ, to the shear and contact waves. There is no justification, physical or mathematical, for doing this. It would appear that the extra dissipation added by this method is sufficient to prevent the Mach stem from kinking.

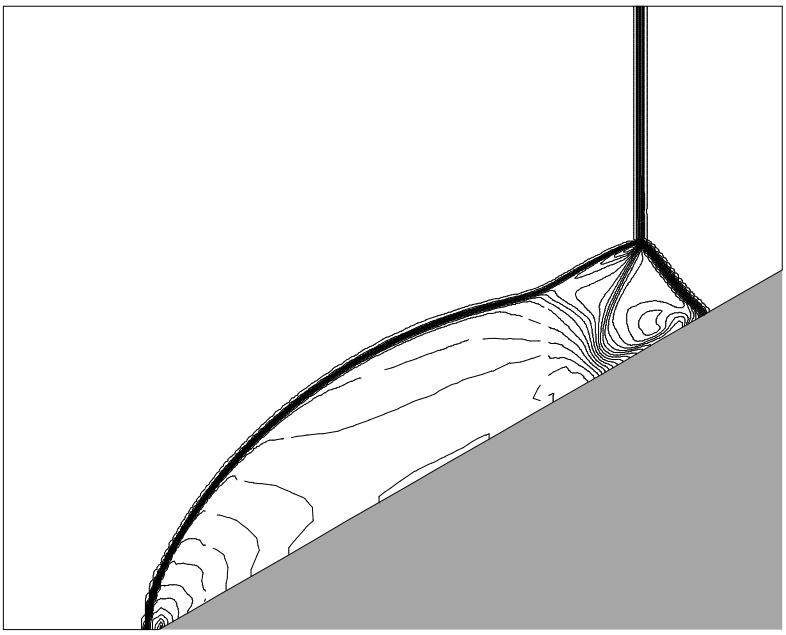

Figure 5.8: DMR; Modified Roe scheme with MinMod limiter function.

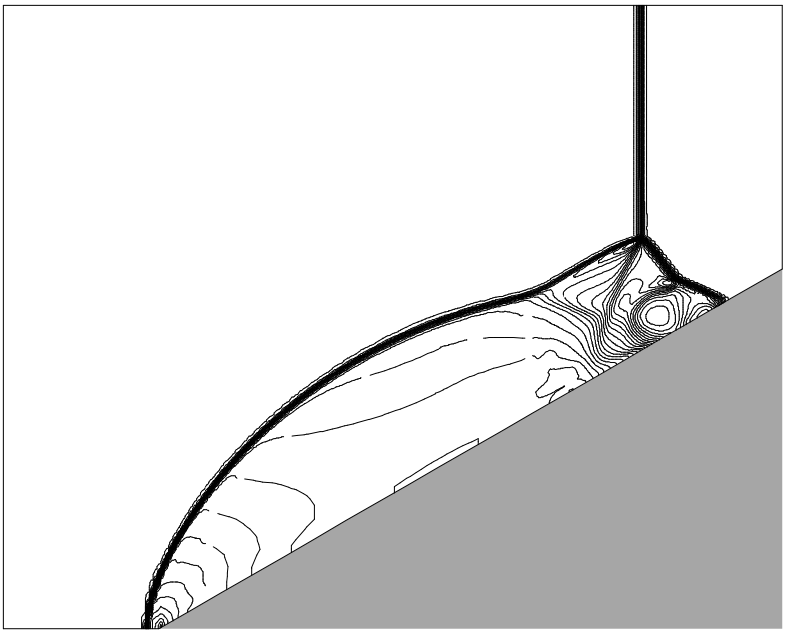

Figure 5.9: DMR; Standard Roe scheme with MinMod limiter function.

5.5 Closing Comment

This chapter contains much information that will be familiar to aficionados of Riemann solvers. Whilst this material may be well worn, enough subtleties remain to justify its inclusion. In particular, given the assumption that waves travel normal to cell interfaces then it is often thought that the extension of a one-dimensional Riemann solver to two-dimensions is straightforward, even trivial. We have shown that this is not necessarily the case. Indeed, for Roe's approximate Riemann solver the mode of failure that we have attributed to an incorrect treatment of the shear wave is so severe as to possibly preclude the use of the scheme for computing certain types of problem. But this would be a pity since in other respects the scheme's robustness and high resolution balanced against the required computational effort is incomparable. Moreover, the trigger for this mode of failure will generally be confined to a very small part of the computational domain. Now, there are two approaches that could be adopted in an attempt to overcome this problem. First a *shear fix* could be added to the standard scheme; we have done this, but have not yet demonstrated its general applicability. Second, an alternative Riemann solver could be used in those regions of the flow domain that are likely to cause problem. In the short term, the extension of this latter approach to include a whole hierarchy of different Riemann solvers could be more effective at preventing the gamut of spurious solutions than the application of numerous *fixes* to any one scheme. But in the long term, genuine multi-dimensional Riemann solvers must surely be a better approach because they will mimic the physics of the flow more closely.